Journal of Microelectronics and Electronic Packaging (2024) **21**, 20–24

ISSN: 1551-4897

Transforming WLP Applications: Introducing Cutting-Edge Next-Generation Nanotwinned Copper Processes to Revolutionize Hybrid Bonding

Pingping Ye*, Jianwen Han, Stephan Braye, Kyle Whitten, Veronica Hayes, Harshul Khanna, Adam Letize, Thomas Richardson, and Elie Najjar

***Abstract*—We discuss two electrochemical plating approaches for nanotwinned copper (ECP nt-Cu)—Gen 1 and Gen 2. These two approaches allow control over columnar width and transition layer thickness on Cu substrates, enabling the filling of nanotwinned Cu for bonding applications. Both approaches produce stable nt-Cu structures with minimal transition layers when electroplated on (111) Cu substrate. However, grain size, transition layer thickness on polycrystalline substrates, and feature-filling behavior differ. The researchers suggest that the choice between Gen 1 and Gen 2 depends on the feature size, aspect ratio, and applications. In addition, further exploration into other additives improves bottom-up filling capabilities, enabling more versatility for applications. Both approaches enable the filling of nanotwinned Cu inside bottom-seeded and complete-seeded features, with 100% nanotwin growth parallel to the substrate for bottom-seeded features. However, nanotwin growth percentage and direction depend on feature size and aspect ratio for complete-seeded features. Gen 2 tends to have less sidewall growth due to its smaller grain size and is more compatible with other additives, making it promising for high aspect ratio small features.**

***Keywords*—Nanotwinned Cu, hybrid bonding, WLP**

Introduction

Heterogeneous integration of wafer-level packaging enables more I/O counts on smaller footprints with shrinking feature sizes and pitch sizes [1]. The interconnect technology evolved from C4 bump, C2 bump, and micropillar with SnAg cap into the most advanced Cu-Cu direct bonding or hybrid bonding without solder cap for high density 2.5D and 3D packaging [2, 3]. Sony utilized this Cu-Cu bonding for its image sensor applications, and AMD partners with TSMC, using hybrid bonding for its 3D V-Cache device [4, 5]. However, current bonding technology requires elevated bonding temperature above 300°C. This temperature is too high and unsuitable for sensitive memory applications like HBM. Nanotwinned Cu (nt-Cu) possesses a unique structure with a high density of twin boundaries embedded in the grain. It can offer lower temperatures for the Cu-Cu direct bonding because its (111) plane-dominated texture has higher atomic diffusivity, leading to a lower thermal budget [6-10]. It also possesses excellent mechanical properties and better electromigration resistance, crucial for device reliability [11-15].

This paper reports two nt-Cu electrochemical plating chemicals: Gen 1 and Gen 2. Both nt-Cu generations produce stable nt-Cu structures with minimal transition layers when electroplated on (111) Cu substrate. However, the difference lies in their grain size, transition layer thickness on polycrystalline substrates, and feature-filling capability. We will elucidate the similarities and differences between these two nt-Cu generations and their applications for various features of WLP, especially potentially for smaller via with a high aspect ratio.

The manuscript was received on November 13, 2023; revision received on January 24, 2024; accepted on February 3, 2024.

The original version of this paper was presented at the 56th International Symposium on Microelectronics (IMAPS'2023), San Diego, CA, USA, October 3-5, 2023.

MacdermidAlpha, 60 Parrott Drive, Shelton, Connecticut

*Corresponding author; email: pingping.ye@macdermidalpha.com

Material and Methods

A. Plating Chemical and Apparatus

The basic makeup solution consists of copper sulfate, sulfuric acid, and hydrochloric acid for chloride ions. The plating bath includes makeup solutions and single or multiple proprietary organic additives. We utilize VSP Biologic Potentiostat to perform coupon-level testing with a mini-cell and water jacket. A water bath controls the plating temperature at 25°C. The anode is an insoluble Titanium anode. The plating current density ranges from 3 to 6 ASD, and the agitation is 100 to 300 rpm.

B. Microstructure and Mechanical Characterization

We observed the electroplated nanotwin microstructure using a dual beam focus ion beam (FIB, Zeiss, Auriga). We characterized the film's texture using x-ray diffraction (XRD, Bruker AXS, D8 discovered with VÅNTEC-500 area detector). Further, we characterized the texture and the grain size using electron backscattered diffraction (EBSD, EDAX). We performed the tensile test with the Instron 5567 at a strain rate of 0.2 in. per minute with a gauge length of 2 in. per IPC-TM-650 standard and measured the internal stress with 1194 Cu alloy test strips per ASTM Standard B975. We also utilized nanoindentation to measure the film strength and hardness per ASTM Standard E2546 (iNano, KLA). Secondary-ion mass spectrometry determines the impurity of plated nt-Cu.

Results and Discussion

A. Gen 1 Nanotwinned Cu

We formulated Gen1 nt-Cu with a single additive in an acidic makeup solution with expansive operating windows, including concentration, agitation, and current density [16, 17]. Fig. 1 shows one example of 4-μm thick nt-Cu film plated on blanket PVD Cu with a direct current of 6 ASD and agitation of 300 rpm at room temperature of 25°C. The single additive concentration is 4 mL/L. The SEM surface image shows 100% nt-Cu coverage on the surface. The grain size is distributed uniformly across the surface. FIB cross-section further confirms that 100% nt-Cu grain throughout the coating depth with barely any transition layer between the Cu seed layer and the nt-Cu structure. One of the attributes of nt-Cu for the low-temperature Cu hybrid-bonding application is the high diffusivity rate of Cu (111), enabling a low thermal budget during the bonding process [6-9]. Both XRD and EBSD indicate that Gen 1 nt-Cu with Cu (111) lattice plane paralleled to the Cu seed. We also demonstrate that the Gen 1 nt-Cu structure is very stable even after annealing at 400°C for 2 h. Fig. 2 shows the FIB cross-section images of nt-Cu annealing at 200, 300, and even 400°C for 2 h. The nt-Cu structure upholds under all these annealing conditions. Literature shows that nt-Cu performs better in electromigration [13-15], and this stable nt-Cu structure in a wide range of temperatures benefits the device's electromigration resistance. In addition to the stable structure, the coating impurity is low. Organic inclusion is only 10 ppm, including C, O, Cl, S, and N. The low impurity is associated with low resistivity and, in some cases, resistance to electromigration; therefore, it is exceptionally critical to device reliability. Using Four Point Probe, we measured the resistivity of 5-μm thick nt-Cu film. The current density is 3 and 6 ASD, and the annealing conditions are at 100, 200, 300, and 400°C for 30 min under forming gas. Fig. 3 shows all measured resistivity is in the range of 17-18 n·Ω·m, which is close to the standard bulk Cu of 17.2 n·Ω·m.

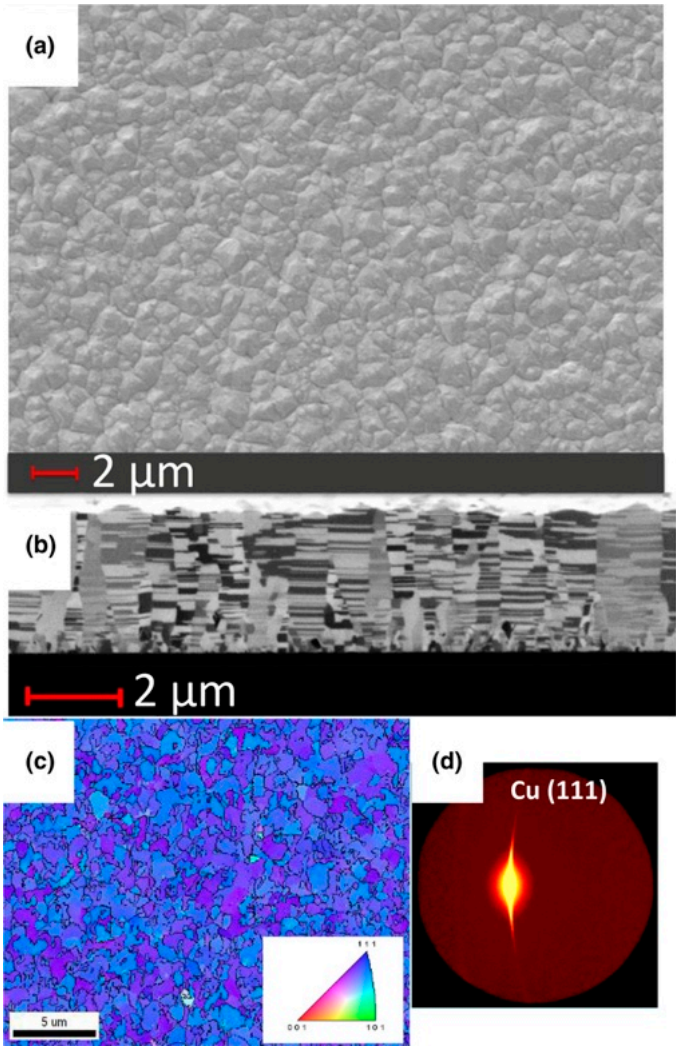

Fig. 1. (a) Surface image, (b) FIB cross-section image, (c) Plan-view EBSD image, (d) 2D XRD diffraction frame with preferred (111) orientation.

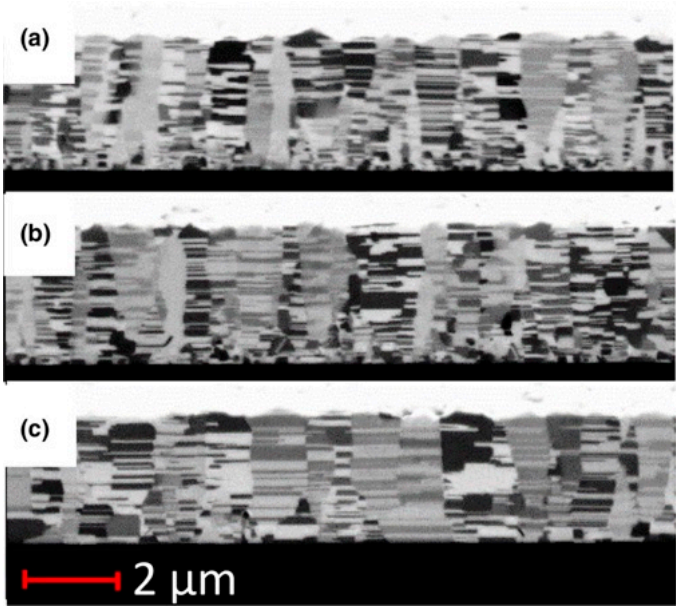

Fig. 2. FIB cross-section images of Gen 1 nt-Cu annealed at elevated temperature for 2 h (a) annealed at 200°C, (b) annealed at 300°C, (c) annealing at 400°C.

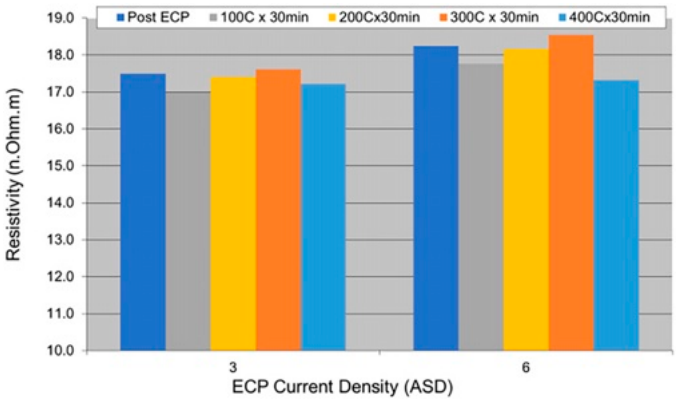

Fig. 3. Resistivity of Gen 1 nt-Cu annealing at various temperatures for 30 min.

B. Comparison of Gen 1 and Gen 2 Nanotwinned Cu

In the last section, we introduced our Gen 1 nt-cu, which enables the formation of 100% nt-Cu with a columnar structure and less than 100-nm thick transition layer on the commercial PVD Cu seed on Si wafer. This Gen 1 nt-Cu can fill different WLP bottom-seeded features, such as pad, pillar, and RDL line. By incorporating a secondary additive, Gen 1 nt-cu can even fill the via with tapered recess, resulting in a high percentage of nt-Cu parallel to the bottom seed of a flat surface [17]. However, for features with the completed seed, such as the damascene structure, there is intense competition between the sidewall direction growth and bottom-up direction growth, as shown schematically in Fig. 4. Therefore, the conformal plating alone process cannot meet the requirement for a high percentage of nt-Cu growing from the bottom when the feature diameter is smaller than 2-3 μm, and the aspect ratio is more significant than 1. Fig. 5 shows Gen 1 nt-Cu filling performance on the trench with a width of 20, 10, 5 μm, down to 2 μm and an aspect ratio from 0.1 to 1. For the broader feature with a low aspect ratio, a high percentage of nt-Cu grows from the bottom, with over 90% of the feature demonstrating nt-Cu parallel to the bottom seed for the 20 and 10 μm width feature shown in Figs. 5a and 5b. For the 5 μm feature, the percentage of nt growing from the bottom decreases to 60%. And for even smaller features (less than 2-3 μm) with a high aspect ratio (more than 1), the percentage of bottom-up growth of nt-Cu decreases significantly to 25%. It becomes more challenging for vias with surrounding sidewalls. There is a need to develop an additive system to promote bottom-up nt-Cu growth while inhibiting sidewall growth to meet the demand for shrinking feature size and pitch size. However, in many cases, adding secondary and third additives into the nt-Cu suppressor-only bath will disrupt the nt-Cu formation, and, in some cases, it will inhibit the bath's nt-Cu formation capability. Therefore, we develop the Gen 2 suppressor.

Despite differences in the additives' nature, there are similarities between Gen 1 and Gen 2. For example, both Gen 1 and Gen 2 have a minimal transition layer when electroplated on (111) dominated Cu substrate and produce very stable (111) dominated nt-Cu structures that are maintained even after 300°C annealing for 4 h. The main differences lie in the grain size (nt-Cu Column width), transition layer thickness plated on polycrystalline substrates, the resistance to nt-Cu disruption with additional accelerator or combination of accelerator and leveler, and associated feature-filling behaviors.

The Gen 2 suppressor produces a smaller grain size and narrower columnar structure than Gen 1. Fig. 6 FIB/SEM and EBSD images indeed show that. The average grain size measured from

Fig. 4. Schematic pictures of simulation growth of grains occurring from both bottom (vertical growth) and side walls (horizontal growth) generate nt-Cu in different orientations.

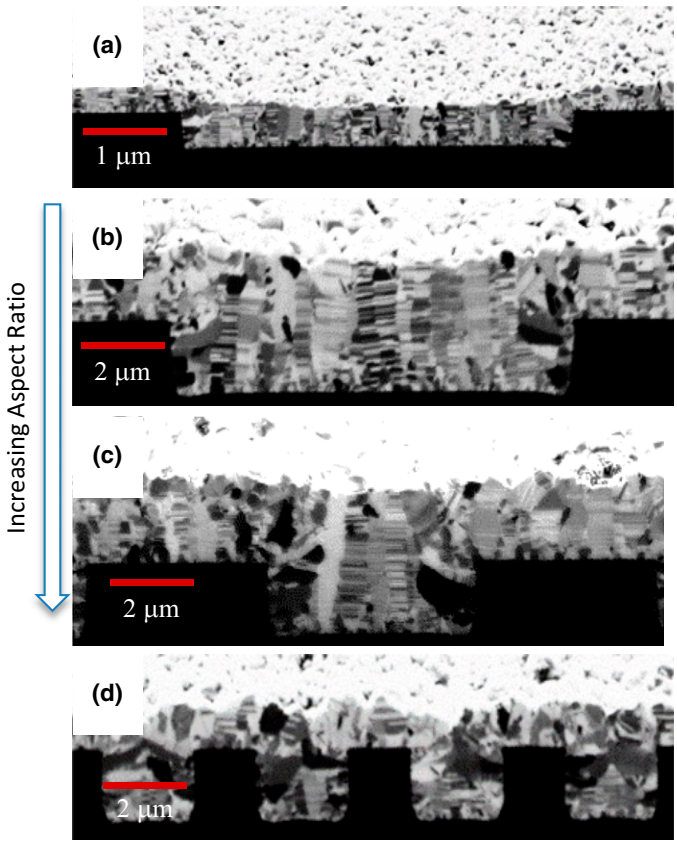

Fig. 5. FIB cross-section of Gen 1 on trench with completed seed with decreasing line width and increasing aspect ratio.

EBSD is that the grain size of the Gen 2 suppressor is about 340 nm, while Gen 1 is 500 nm. Different grain sizes change the measured ultimate tensile strength, as shown in Fig. 7. Strips were grown 25 μm thick for pulling. The smaller-grained Gen 2 chemistry demonstrates the ultimate tensile strength of 470 MPa, while Gen 1 demonstrates the ultimate tensile strength of 290 MPa. Per the standard tradeoff between ductility and strength, Gen 2 shows failure at yield for the elongation of 2%, while Gen 1 shows hardening after yield for the elongation of 11%. These results are commensurate with the expectation that smaller grains yield increased strength [18-20]. Nanoindentation

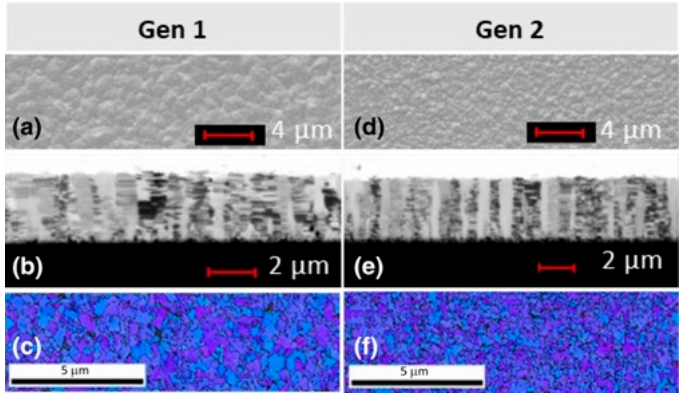

Fig. 6. (a, b, and c) Gen 1 surface, FIB cross-section, and EBSD image; (d, e, and f) Gen 2 surface, FIB cross-section and EBSD image.

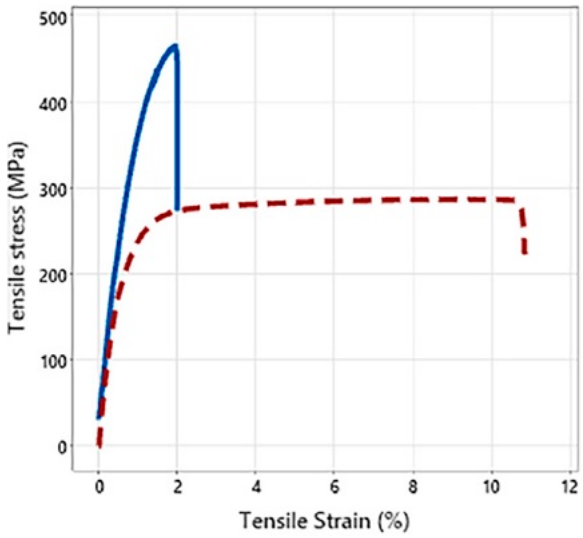

Fig. 7. Comparison of tensile properties of Gen 1 (red) to Gen 2 (blue) for 25-μm thick test strips.

measurements, as shown in Fig. 8, also support these results. The Young's modulus of Gen 1 and Gen 2, calculated from the unloading curve, is 155 and 165 GPa, and their nano hardnesses are 2.00 and 2.482 GPa, respectively. The internal stress measured with 1,194 Cu alloy test strips is less than 20 Mpa for Ge1 1 and Gen 2. The improved mechanical properties are attractive for semiconductor devices to decrease warpage during device fabrication.

The second difference between Gen 1 and Gen 2 is the transition layer thickness when plating on a polycrystalline Cu substrate. Fig. 9 shows the 4-μm thick Cu film plated on (111) dominated PVD Cu seed or polycrystalline Cu seed. Gen 1 and 2 can produce nt-Cu on (111) dominated Cu seed with a shallow transition layer. EBSD shows more than 99% of (111) plane parallel to the substrate. However, for polycrystalline Cu seed, Gen 2 can produce nt-Cu with a shallow transition layer,

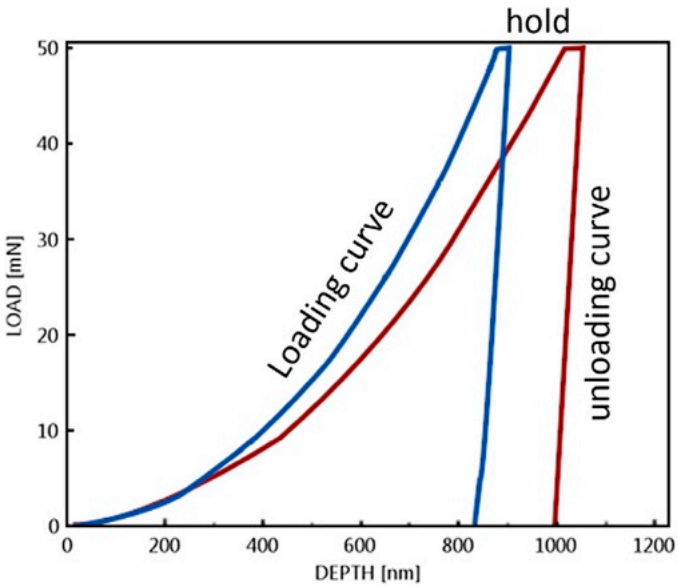

Fig. 8. Load-depth curve of nano-indentation of Gen 1 (red) and Gen 2 (blue).

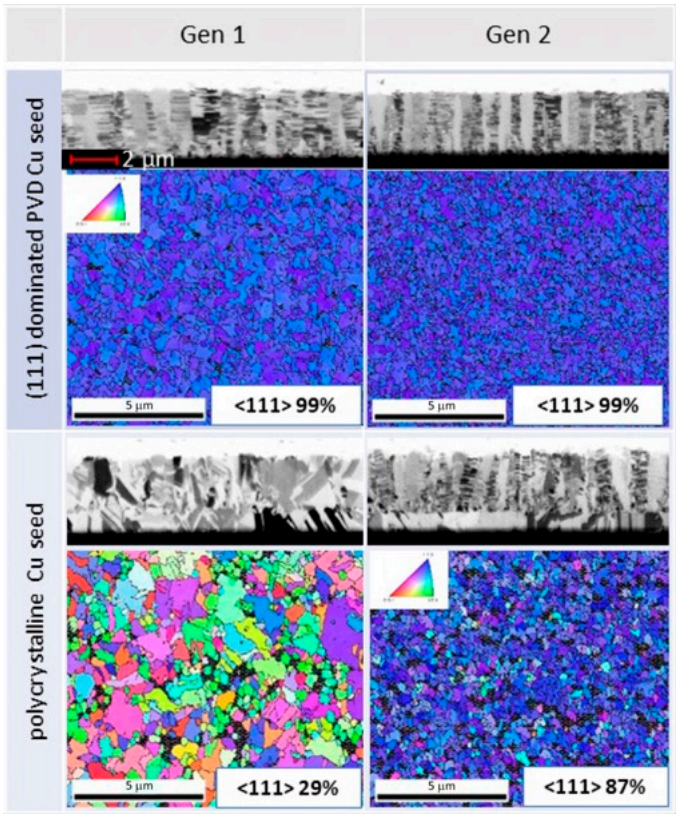

Fig. 9. Comparison of nt-Cu formation capability of Gen 1 and Gen 2 on polycrystalline substrate.

and Gen 1 leads to a higher transition layer. EBSD also shows that Gen 2 produces nt-Cu with more than 87% of (111) plane parallel to the substrate. For Gen 1, it is about 29%. With increasing plating time, the thick film will produce more nt structure. Therefore, the main difference is the transition layer thickness. This technique provides two approaches for a two-step process for a high aspect ratio, as shown in Fig. 10. The first step is the bottom-up process to decrease the aspect ratio to have more nt-Cu grow vertically from the bottom in the second step. However, Cu texture could be (111) dominated or none (111) dominated for this first step of the bottom-up process. In the case of a nondominated Cu first-step process (111), if a low transition layer is essential in the second step, Gen 2 will be the preferred choice. In other cases, where the first step is (111) dominated surface or low transition layer for the second step is not critical, Gen 1 and Gen 2 are suitable.

Another difference between these two nt-Cu generations is the resistance to nt-Cu disruption by adding a secondary or

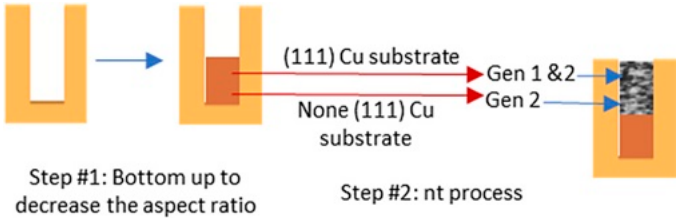

Fig. 10. Schematic graph showing choice of Gen 1 and Gen 2 for two-step process.

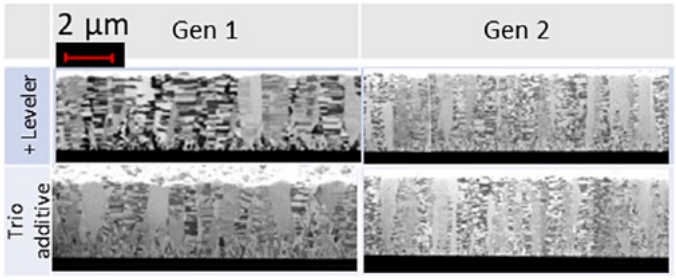

Fig. 11. Comparison of nt-Cu formation capability of Gen 1 and Gen 2 with addition leveler/accelerator (SPS).

third additive into the plating bath. Fig. 11 shows the nt-Cu formation ability by adding a leveler or accelerator and leveler into the plating bath. The electroplated film thickness is 4 µm. For Gen 1 and 2, the additional proprietary leveler and accelerator in the plating bath will produce nt-Cu. There is barely any transition layer for Gen 2. The plating bath can maintain the ability to produce 100% of the fine nt-Cu structure. XRD further confirmed the plated film is nt-Cu with more than 99% of (111) plane parallel to the substrate. This trio additive system provides the possible approach to boost the bottom-up fill for a high aspect ratio and small opening.

Conclusion

We demonstrated two electrochemical nt-Cu plating approaches, Gen 1 and Gen 2, for hybrid-bonding applications. Both Gen 1 and Gen 2 have a minimal transition layer when electroplated on (111) dominated Cu substrate and produce very stable (111) dominated nt-Cu structures even after 300°C annealing for 4 h. Gen 1 nt-Cu can fill different WLP features with the bottom and completed seed. However, it is challenging for the completed seed features with a diameter of less than 2-3 µm and an aspect ratio larger than 1. One of the methods is a two-step plating process. In the case of none (111) dominated Cu first-step process and the requirement of a low transition layer in the second step, Gen 2 will be the preferred choice. In other cases, where the first step is (111) dominated surface or low transition layer for the second step is not critical, Gen 1 and Gen 2 are suitable. The other method is the trio-additives system.

Acknowledgments

The authors thank our marketing team, Brian Gokey, for discussing the nt-Cu for hybrid-bonding applications and providing customers' feedback. The authors also thank our Taiwan WLP application lab for their support.

References

[1] J.H. Lau, *Semiconductor Advanced Packaging*, Springer, 2021.
[2] L. Mirkarimi and G. Gao, "Die-to-wafer hybrid bonding for 2.5D and 3D integration," *Chip Scale Review*, pp. 29-35, March and April 2020, https://www.chipscalereview.com/issues/ChipScale_Mar-Apr_2020-digital.pdf.
[3] https://semiengineering.com/hybrid-bonding-basics-what-is-hybrid-bonding/.
[4] H. Tsugawa, H. Takahashi, R. Nakamura, T. Umebayashi, T. Ogita, H. Okano, K. Iwase, H. Kawashima, T. Yamasaki, D. Yoneyama, J. Hashizume, T. Nakajima, K. Murata, Y. Kanaishi, K. Ikeda, K. Tatani, T. Nagano, H. Nakayama, T. Haruta, and T. Nomoto, "3.2 pixel/DRAM/logic 3-layer stacked CMOS image sensor technology," 2017 IEEE International Electron Devices Meeting (IEDM), pp. 3.2.1-3.2.4, San Francisco, CA, 2-6 December 2017.
[5] https://www.anandtech.com/show/16725/amd-demonstrates-stacked-vcache-technology-2-tbsec-for-15-gaming.
[6] J.-Y. Juang, C.-L. Lu, K.-J. Chen, C.-C.A. Chen, P.-N. Hsu, C. Chen, and K.N. Tu, "Copper to copper direct bonding on highly (111)-oriented nanotwinned copper in no-vacuum ambient," *Scientific Reports*, Vol. 8, pp. 13910, 2018.
[7] C.-M. Liu, H.-W. Lin, Y.-S. Huang, Y.-C. Chu, C. Chen, D.-R. Lyu, K.-N. Chen, and K.-N. Tu, "Low-temperature direct copper-to-copper bonding enabled by a creep on (111) surfaces of nanotwinned Cu," *Scientific Reports*, Vol. 5, pp. 9734, 2015.
[8] P. Gondcharton, B. Imbert, L. Benaissa, V. Carron, and M. Verdier, " Kinetics of low-temperature direct copper-copper bonding," *Microsystem Technologies*, Vol. 21, pp. 995-1001, 2015.
[9] W. Chiu, O. Lee, and C. Chiang, "Low-temperature wafer-to-wafer hybrid bonding by nanotwinned copper," 2021 IEEE 71st Electronic Components and Technology Conference (ECTC), pp. 365-370, San Diego, CA, 1 June-4 July 2021.
[10] L. Mirkarimi, C. Uzoh, D. Suwito, B. Lee, G. Fountain, T. Workman, J. Theil, and G. Gao, "The influence of Cu microstructure on thermal budget in hybrid bonding," 2022 IEEE 72nd Electronic Components and Technology Conference (ECTC), pp. 162-167, San Diego, CA, 31 May-3 June, 2022.
[11] L. Lu, X. Chen, X. Huang, and K. Lu, "Revealing the maximum strength in nanotwinned copper," *Science (New York, N.Y.)*, Vol. 323, pp. 607-610, 2009.
[12] L. Lu, Y. Shen, X. Chen, L. Qian, and K. Lu, "Ultrahigh strength and high electrical conductivity in copper," *Science (New York, N.Y.)*, Vol. 304, pp. 422e6-426, 2004.
[13] I. Tseng, K. Shie, B. Hung, C. Chang, and C. Chen, "Electromigration in 2 µm redistribution lines and Cu-Cu bonds with highly 111 oriented nanotwinned Cu," 2020 IEEE 70th Electronic Components and Technology Conference (ECTC), pp. 479-484, Lake Buena Vista, FL, May 26-29 2020.
[14] F. Shen, C. Huang, Y. Lo, W. Hsu, C. Wang, and C. Chen, "Atomic-scale investigation of electromigration with different directions of electron flow into high-density nanotwinned copper through in situ HRTEM," *ActaMater*, Vol. 219, pp. 117250, 2021.
[15] Y. Kuo, D. Tran, J. Ong, K.N. Tu, and C. Chen, "Hybrid Cu-to-Cu bonding with nanotwinned Cu and non-conductive paste," *Journal of Materials Research and Technology*, Vol. 18, pp. 859-871, 2022.
[16] P. Ye, J. Han, S. Braye, K. Whitten, R. Hurtubise, T. Richardson, and E. Najjar, "Electrochemical plating of nanotwinned Cu for WLP applications," Proceedings of the International Wafer Level Packaging Conference (it is a virtual meeting due to the covid) San Jose, CA, 13-30 October 2020. DOI: 10.23919/IWLPC52010.2020.9375876
[17] J. Han, P. Ye, S. Braye, K. Whitten, C. Wang, D. Shaffer, A. Letize, B. Gokey, T. Richardson, and E. Najjar, "Electrochemical plating system development of nanotwinned Cu for multiple WLP features," IMAPS 18th Conference, Fountain Hills, Arizona USA March 7-10, 2022.
[18] S. Chung, Y.-T. Chen, and Z.-C. Chen, "Electroplated nanotwin copper for fine line RDL," 2018 China Semiconductor Technology International Conference (CSTIC), pp. 1-3, Shanghai, China, 11-12 March 2018.
[19] N.J. Simon, E.S. Drexler, and R.P. Reed, "Properties of copper and copper alloys at cryogenic temperatures," *NIST Monograph*, Vol. 177, 1992.
[20] Z. Yang, L. Zheng, Y. Yue, and Z. Lu, "Effects of twin orientation and spacing on the mechanical properties of Cu nanowires," *Scientific Reports*, Vol. 7, pp. 10056, 2017.